Location of pointlike acoustic emission sources in anisotropic plates

Bernard Castagnede, Wolfgang Sachse and Kwang Yul Kim

Citation: The Journal of the Acoustical Society of America **86**, 1161 (1989); doi: 10.1121/1.398110
View online: https://doi.org/10.1121/1.398110
View Table of Contents: https://asa.scitation.org/toc/jas/86/3
Published by the Acoustical Society of America

Location of pointlike acoustic emission sources in anisotropic plates

Bernard Castagnede, Wolfgang Sachse, and Kwang Yul Kim
Department of Theoretical and Applied Mechanics, Cornell University, Ithaca, New York 14853

(Received 8 February 1989; accepted for publication 18 May 1989)

In this paper is described a method by which a pointlike source of acoustic emission can be located in an anisotropic plate. The method is applicable for a source in an anisotropic solid of arbitrary symmetry as long as the principal acoustic axes of the material are known *a priori*. It is shown that from the time-of-flight differences of particular features in the waveforms detected by any pair of sensors, a set of nonlinear transcendental equations can be formed in which the coefficient of each term in the equations is related to the time-of-flight differences, the geometrical parameters of the array, and the wave speeds of quasiwaves propagating along each source/receiver path. For waves propagating in principal planes, the analytical expressions for the wave speed values are used. Extension to nonprincipal planes is obtained by computing the eigenvalues of the Green–Christoffel tensor. Determination of the optimum location of the source is found by minimizing the Euclidean functional associated with the set of transcendental nonlinear equations. The results obtained with numerical simulations of two- and three-dimensional source-location problems are presented to illustrate several characteristic features of the solution. Also shown are the results of two-dimensional source-location measurements made on specimens of a unidirectional fiber-glass-reinforced composite material. The results demonstrate the efficiency of the algorithm in locating a source of emission.

PACS numbers: 43.20.Rz, 43.40.Ph

INTRODUCTION

The problem of locating a source of acoustic emission in a structure is of importance in geophysics as well as nondestructive materials testing. To solve this problem, knowledge is needed about the radiation characteristics of the source, the propagation of the elastic waves between the source and the receivers, and the geometry of the receiving sensor array. The solution of this problem for the most general case is enormously difficult. In actual applications, simplifications are sought to obtain a solution. When the source is small compared to the source–receiver separation, the material is homogeneous and isotropic, and the sensors are pointlike and are positioned in a geometrical configuration, considerable simplifications result in the analytical and numerical treatment. The assumptions used must, however, be physically realistic for particular measurement situations. In seismology, the earth's crust possesses discontinuities and gradients in its mechanical properties.[1] To describe the propagation of elastic waves in the earth, very special analytical methods have been utilized, and the location of seismological sources relies on numerical procedures utilizing complex algorithms which are modified with succeeding events.[1] For the study of materials and, in particular, the dynamics of failure processes and wave interactions in them, the quantitative acoustic emission (QAE) technique has been developed. The basis of the technique is that a source in a material emits elastic waves which are detected at the surface of the structure and AE signal-processing techniques are then used to process these signals to identify and to characterize the source of emission. The source corresponds to a dynamic force field change and an irreversible release of energy at the source point. It may be the result of the motions of dislocations, the initiation and propagation of a crack, phase transformations, or the action of simulated sources such as the thermoelastic and ablative effects accompanying the interaction of a laser or similar source and a material (cf. Ref. 2). The first and essential requirement is to locate the source of emission. This paper is restricted to this problem and, in particular, to the case of a source in an anisotropic material.

All source location techniques rely on measurements of the arrival time of a particular wave mode at a sensor. The measurement can be made directly by time-interval electronic measuring counters, or indirectly from analysis of digitized waveforms via their Fourier phase function or a correlation analysis. It is recognized, however, that in many practical situations, errors arise from multiple events and background noise. Also, arrival-time measurements are prone to errors because of wave attenuation, scattering, and material and geometric dispersion effects, some or all of which are present in real materials.[3]

To overcome these difficulties, various modified source-location techniques have been proposed. Included are the *approximate zone location* and *hit sequence* techniques by which the sensor or the small number of sensors at which the first arrival of an AE signal define a region of a structure in which the AE source is located. While these do not give an exact location, they appear to work well in highly absorbent materials.[3] For locating pointlike acoustic emission sources in homogeneous isotropic solids, triangulation methods[4] are generally used. These approaches are extended to different geometries,[5] and might also include least-squares numerical techniques[6] and correlation methods.[7,8]

If the source of emission is located at $\mathbf{x}^S$, i.e., (x_1^S, x_2^S, x_3^S)

 0001-4966/89/091161-11$00.80

in a structure and the AE is detected by N sensors whose location is specified by $\mathbf{x}^k$ ($k = 1,2,3,...,N$), then the distance between the k th sensor and the source can be determined from measurements of the arrivals, t^k, of particular waves at the sensor, given by

$$D^k = \sqrt{(x_1^k - x_1^S)^2 + (x_2^k - x_2^S)^2 + (x_3^k - x_3^S)^2}, \quad (1)$$

and

$$D^k = (t^k - t_0)c, \quad (2)$$

where c is the speed of propagation of the wave and t_0 is the unknown time origin of the source. Since there are also the three unknown source coordinates, the arrival times determined from the waveforms detected at four sensor positions are required to uniquely locate a source. It is advantageous to use more than four sensors since the system of equations becomes over determined and least-squares processing algorithms can be used to obtain the optimal solution to the measured arrival-time data.[9] Critical to the above procedure is knowledge of the speed of propagation of a particular wave mode. Unfortunately, because of geometric wave-dispersion effects, the identification of wave arrivals of equivalent wave modes in signals detected by sensors located at widely different distances from the source point becomes difficult. This has led to the development of a small-array sensor[10] for which the source of emission is always exterior to the array. For this case, the source-location procedure can be based on measurement of the arrivals of two dominant pulses in a waveform whose speeds of propagation, c_1 and c_2, are known. If the time difference between the two modes detected at the k th sensor is specified by Δt_{12}^k, then the range to the source from that sensor is given by

$$D^k = \Delta t_{12}^k [c_1 c_2/(c_1 - c_2)]. \quad (3)$$

The angle between the axis of the array and the source is subsequently found by triangulation.

To be able to simulate numerically various causes of systematical errors in the source-localization process, statistical methods have been extensively used. For instance, staggering the positions of the sensors,[11] the presence of noise,[12] and the dispersive nature of signals in guided geometries[13] have all been studied. Furthermore, some systems that accomplish the task of locating an AE source in isotropic materials in a simple manner have been described.[10,14]

Determination of the location of a source of emission in an anisotropic material is complicated by the fact that the speed of propagation of each wave mode is dependent on the propagation direction in the material. While it has been recognized that a solution of this problem is of importance in successfully using AE measurements in anisotropic materials, such as in structures fabricated of composite materials, it has not been possible to do so until recently.[15] Our initial contribution in obtaining a solution to this problem included a preliminary experiment which clearly demonstrated the correctness of the basic algorithm with real data.[16] We report here on new results and give a detailed description of the method. Also, we include extensions of the location process to the full three-dimensional source-location problem. To ascertain some features as well as some inherent limitations of the solution for a general anisotropic medium, numerical simulations have been extensively used. The general solution of the basic localization problem of a pointlike source in an arbitrary anisotropic plate is discussed in the following section. The use of numerical simulations for the two- and three-dimensional cases are discussed in Sec. II. Then, in Sec. III are presented experimental data for a unidirectional composite material. This is followed by concluding remarks in Sec. IV.

I. GENERAL SOLUTION OF THE 3-D SOURCE-LOCATION PROBLEM

The solution of the general three-dimensional source-location problem in an anisotropic solid is a formidable task. Here, we restrict ourselves to a simpler problem by adopting the following assumptions: (1) We suppose that the wave propagation occurs in an infinite platelike structure whose thickness is uniform; (2) the material is a perfectly elastic, homogeneous anisotropic solid; (3) the wave dispersion is negligible; (4) the active areas of the source as well as the receivers are pointlike; (5) the order of the elastic symmetry of the solid is restricted to be orthorhombic or higher; and (6) the principal axes of the solid are known *a priori* and are oriented along the coordinate axes of the specimen.

The first assumption is often readily realized in practice since platelike elements are very common structural components. The second assumption, which is indirectly linked to the third one, might appear somehow restrictive because perfectly elastic bodies are rare, especially when applications in the field of synthetic materials such as composites are considered. Our approach here is to describe a basic problem in a very general way. For that purpose, we need to make several simplifications, and the absence of dispersion will be one of them. It may be possible to include the influence of dispersion in the treatment, and this point will be addressed later. The fourth assumption is met by many actual sources of emission and by using small aperture sensors to detect the signals. By definition, a pointlike source or a receiver is one whose active region is small compared to the sensor/source separation and whose dimension is smaller than the dominant wavelength in the AE signal. In many applications this assumption is easily met. Excluded from our analysis are very small arrays of receiving sensors for which the source is located exterior to the array. Also excluded are extended sources. It may be possible to extend the method described here to such sources, but this will not be developed further here. The last two assumptions are often made in describing the mechanics of composite materials. Most engineering materials are characterized by high-symmetry order in their elastic properties. Generally, an orthorhombic symmetry is sufficient to describe the properties. The last assumption, which involves the superposition of the geometric and crystallographic axes, can always be verified by a preliminary calibration procedure.

The placement of the sensors comprising the receiving array is of considerable importance. In some cases, the sensors are positioned on one or both surfaces of the test specimen and the surfaces themselves correspond to a principal plane of the material. This is usually the case for nearly all engineering sheetlike materials, and such a testing situation

is not too restrictive. On the other hand, the last assumption is inappropriate when making measurements on single-crystal specimens which have been cut in an arbitrary orientation. Thus the method that is proposed here is intrinsically limited to ordinary engineering materials.

Dealing only with that last case, several configurations for the sensors are possible, in terms of their positioning. Figure 1 describes three common configurations. These include the random distribution, the two orthogonal lines case, and the circular configuration. Each of these arrangements has its advantages and disadvantages. For instance, the random distribution might be of interest when dealing with a stochastic problem, i.e., when the source location might be located at an arbitrary site in the plate. This is similar to the measurements in quantitative seismology. In the testing of materials, however, particular regions of a structure are more critical or, because of the stresses which are applied, are more likely to fail and hence need to be especially monitored. We limit ourselves here in the description of deterministic process only. For this situation, a more regular distribution of the sensors is desirable, and thus the two orthogonal lines and circular distributions are of special interest. The formulation we will analyze in detail will be the circular configuration. However, the calculations for the two-orthogonal lines case are similar but simpler.

We consider an anisotropic, flat plate of thickness $2h$ with the distribution of pointlike piezoelectric sensors over both surfaces. Suppose that a pointlike acoustic emission source S is located in the plate at coordinates x_1^S, x_2^S, and x_3^S as shown in Fig. 2. By selecting a given pair of sensors (k,m),

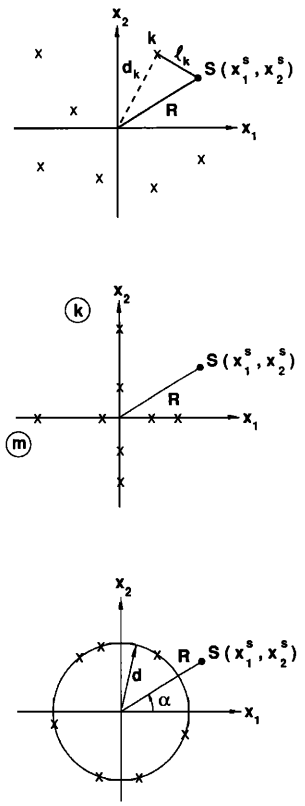

COMMENTS FOR FIGURE 1

(a) General case

$$l_k^2 = R^2 + d_k^2 - 2x_{1k}x_1^S - 2x_{2k}x_2^S,$$

with an analogous expression for l_m, where

$$R^2 = (x_1^S)^2 + (x_2^S)^2,$$

$$d_k^2 = x_{1k}^2 + x_{2k}^2.$$

(b) Two orthogonal lines

$$\begin{cases} l_k^2 = R^2 + x_{2k}^2 - 2x_{2k}x_2^S, \\ l_m^2 = R^2 + x_{1m}^2 - 2x_{1m}x_1^S, \end{cases}$$

where

$$R^2 = (x_1^S)^2 + (x_2^S)^2,$$

with k along axis X_2 and m along axis X_1.

(c) Circular array

$$l_k^2 = R^2 + d^2 - 2\,dx_1^S \cos\alpha_k - 2\,dx_2^S \sin\alpha_k,$$

with an analogous expression for l_m, where

$$R^2 = (x_1^S)^2 + (x_2^S)^2.$$

α_k, α_m: angular coordinates for sensors k,m.

FIG. 1. Various spatial distributions for the array of sensors.

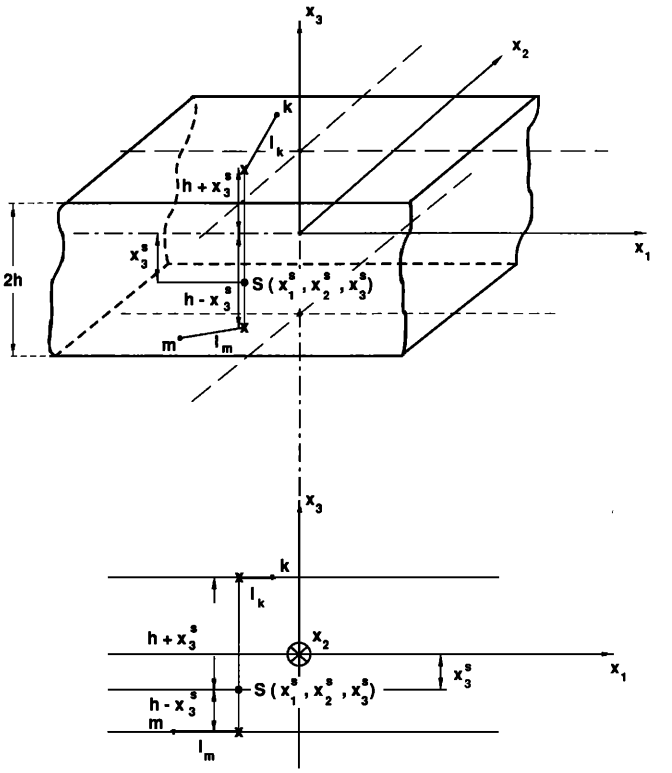

FIG. 2. Geometry in the general case.

where k refers for the sensor positioned on the upper surface and m for a sensor mounted on the bottom surface, a simple time-difference equation between the arrivals of the P-wave arrivals at the two sensors follows from Eqs. (1) and (2):

$$\Delta t_p(k,m) = [c_p(n_k)]^{-1}\sqrt{(h + x_3^S)^2 + l_k^2} - [c_p(n_m)]^{-1}\sqrt{(h - x_3^S)^2 + l_m^2}. \quad (4)$$

Here $k,m = 1,\ldots,N$ with $N > 3$, where N equals the number of sensors on each surface of the structure being monitored. The total number of sensors in this case is $2N$, but this is arbitrary. The quantities l_k and l_m represent the distance between source and sensor k or sensor m projected onto the top or bottom surfaces of the plate, respectively. The wave speeds of the quasilongitudinal wave along the two source/receiver acoustical paths are specified by $c_p(n_k)$, and $c_p(n_m)$, respectively, where n_k and n_m are the corresponding direction cosines of the propagational paths.

The distances l_k and l_m depend on the chosen sensor array geometry and are functions of the respective in-plane coordinates of the source and sensor. Some examples for these quantities are shown in Fig. 1. As stated earlier, the equations to be presented which are relevant to the numerical simulations, as well as the experiments to be described, will be based on the circular array geometry. But the implementation of other geometries is always possible by changing the numerical expressions for l_k and l_m.

The wave speeds $c_p(n_k)$ and $c_p(n_m)$ are functions of the direction cosines n_k and n_m, respectively. The wave propagation is in one of the principal planes in only a few directions of the specimen. If for convenience X_1, X_2 and X_3 are principal axes of symmetry, then the direction cosines are

given by the following expressions for each pair of N sensors, $k,m = 1,2,...,N$:

$$
\begin{aligned}
n_{1,2}^k &= (x_{1,2}^k - x_{1,2}^S)/D, \\
n_3^k &= (h + x_3^S)/D, \\
n_{1,2}^m &= (x_{1,2}^m - x_{1,2}^S)/D', \\
n_3^m &= (h - x_3^S)/D',
\end{aligned} \tag{5}
$$

where

$$
\begin{aligned}
D &= [(h + x_3^S)^2 + (x_1^k - x_1^S)^2 + (x_2^k - x_2^S)^2]^{1/2}, \\
D' &= [(h - x_3^S)^2 + (x_1^m - x_1^S)^2 + (x_2^m - x_2^S)^2]^{1/2}.
\end{aligned}
$$

However, the direction of wave propagation is generally in nonprincipal planes for which there are no analytical expressions for the wave speeds.[17] One needs therefore to compute the eigenvalues of the Green–Christoffel tensor, sometimes called the propagation tensor Γ_{il}, by using the characteristic equation

$$
\det|\Gamma_{il} - \rho c^2 \delta_{il}| = 0, \tag{6}
$$

where $\Gamma_{il} \equiv C_{ijkl} n_j n_k$ and where $(i,j,k,l = 1,2,3)$ with C_{ijkl} is the stiffness tensor of the material. The term ρ is the density of the material, δ_{il} is the Kronecker delta, and c are the wave speeds (quasilongitudinal and quasishear) of the wave propagating in a particular direction in the material. The direction cosines appearing in this equation are identical to those given in Eq. (4) for the top and bottom sensors. For an orthorhombic material, the propagation tensor has the components

$$
\begin{aligned}
\Gamma_{11} &= n_1^2 C_{11} + n_2^2 C_{66} + n_3^2 C_{55}, \\
\Gamma_{22} &= n_1^2 C_{66} + n_2^2 C_{22} + n_3^2 C_{44}, \\
\Gamma_{33} &= n_1^2 C_{55} + n_2^2 C_{44} + n_3^2 C_{33}, \\
\Gamma_{21} &= \Gamma_{12} = (C_{12} + C_{66}) n_1 n_2, \\
\Gamma_{31} &= \Gamma_{13} = (C_{13} + C_{55}) n_1 n_3, \\
\Gamma_{32} &= \Gamma_{23} = (C_{23} + C_{44}) n_2 n_3,
\end{aligned} \tag{7}
$$

where the elastic constants have been written with the conventional abbreviated notation (cf. Ref. 17, p. 64).

The eigenvalues of the Green–Christoffel tensor are computed by using a cyclic Jacobi method with threshold value sweeps.[18,19] Some numerical results using this scheme are presented in Sec. II D. We note that when dealing with thin plates, i.e., the ratios $2h/d$ and $2h/R \ll 1$, and the propagation occurs approximately in one of the principal planes (cf. 1,2).

For example, in the two-dimensional problem in which x_3 is not an unknown, it suffices to mount the sensors onto only one surface of the specimen. In such a case, analytical expressions for the wave speed curves are available for materials of specified elastic anisotropies.[17] For instance, the wave speed for the quasilongitudinal mode of an orthorhombic material in the principal plane (1,2) is given by

$$
c_p(\theta) = \{(1/2\rho)[A(\theta) + \sqrt{A(\theta) - 4B(\theta)}]\}^{1/2}, \tag{8}
$$

where

$$
\begin{aligned}
A(\theta) &= C_{11}\cos^2\theta + C_{22}\sin^2\theta + C_{66}, \\
B(\theta) &= (C_{11}\cos^2\theta + C_{66}\sin^2\theta) \\
&\quad \times (C_{66}\cos^2\theta + C_{22}\sin^2\theta) \\
&\quad - (C_{12} + C_{66})^2 \sin^2\theta\cos^2\theta,
\end{aligned}
$$

with

$$
\theta = \arccos\left(\frac{x_1^k - x_1^S}{\sqrt{(x_1^k - x_1^S)^2 + (x_2^k - x_2^S)^2}}\right). \tag{9}
$$

This equation is applicable for each sensor, i.e., $k = 1,2,...,N$, as shown in Fig. 3.

In the general three-dimensional source-location problem, the time-of-flight measurements result in a system of equations according to Eq. (4). Since there are only three unknown source coordinates, x_1^S, x_2^S, and x_3^S, this system is overdetermined and an optimization technique to efficiently solve this problem can be used.[18] For that purpose, Eq. (4) is rearranged, squared twice, and after some algebraic manipulations one obtains the following set of nonlinear equations:

$$
\begin{aligned}
\Psi(\mathbf{x}^S) &= A_1(x_3^S)^4 + A_2(x_3^S)^3 + A_3 x_1^S (x_3^S)^2 \\
&\quad + A_4 x_2^S (x_3^S)^2 + A_5 (x_3^S)^2 + A_6 (x_1^S)^2 \\
&\quad + A_7 (x_2^S)^2 + A_8 x_1^S x_2^S + A_9 x_1^S x_3^S + A_{10} x_2^S x_3^S \\
&\quad + A_{11} x_1^S + A_{12} x_2^S + A_{13} x_3^S + A_{14} \simeq 0,
\end{aligned} \tag{10}
$$

where $\mathbf{x}^S \equiv x_1^S, x_2^S, x_3^S$ are, as before, the coordinates of the source. The coefficients A_i with $i = 1,2,...,14$ correspond to each (k,m) pair of sensors and they are given by the expressions

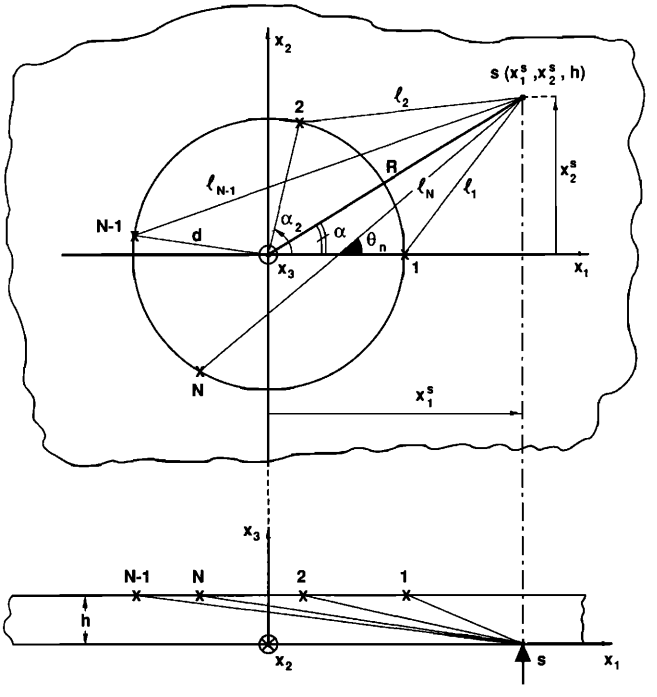

FIG. 3. Detailed geometry for the circular array of sensors.

$$
\begin{aligned}
A_1 &= [c_p^2(\theta_k) - c_p^2(\theta_m)]^2,\\
A_2 &= 4h\,[c_p^4(\theta_k) - c_p^4(\theta_m)],\\
A_3 &= 4d\,[c_p^2(\theta_k)c_p^2(\theta_m)(\cos\alpha_m + \cos\alpha_k)\\
&\quad - c_p^4(\theta_k)\cos\alpha_m - c_p^4(\theta_m)\cos\alpha_k],\\
A_4 &= 4d\,[c_p^2(\theta_k)c_p^2(\theta_m)(\sin\alpha_m + \sin\alpha_k)\\
&\quad - c_p^4(\theta_k)\sin\alpha_m - c_p^4(\theta_m)\sin\alpha_k],\\
A_5 &= 2\{k_a[c_p^2(\theta_k) - c_p^2(\theta_m)]^2\\
&\quad - K_{km}^2[c_p^2(\theta_k) + c_p^2(\theta_m)]\\
&\quad + 2h^2[c_p^2(\theta_k) + c_p^2(\theta_m)]^2\},\\
A_6 &= 4d^2[c_p^2(\theta_k)\cos\alpha_m - c_p^2(\theta_m)\cos\alpha_k]^2,\\
A_7 &= 4d^2[c_p^2(\theta_k)\sin\alpha_m - c_p^2(\theta_m)\sin\alpha_k]^2,\\
A_8 &= 8d^2[c_p^4(\theta_k)\cos\alpha_m\sin\alpha_m + c_p^4(\theta_m)\cos\alpha_k\sin\alpha_k\\
&\quad - c_p^2(\theta_k)c_p^2(\theta_m)\sin(\alpha_m + \alpha_k)],\\
A_9 &= 8hd\,[c_p^4(\theta_m)\cos\alpha_k - c_p^4(\theta_k)\cos\alpha_m\\
&\quad + c_p^2(\theta_k)c_p^2(\theta_m)(\cos\alpha_k - \cos\alpha_m)],\\
A_{10} &= 8hd\,[c_p^4(\theta_m)\sin\alpha_k - c_p^4(\theta_k)\sin\alpha_m\\
&\quad + c_p^2(\theta_k)c_p^2(\theta_m)(\sin\alpha_k - \sin\alpha_m)],\\
A_{11} &= 4d\{K_{km}^2[c_p^2(\theta_k)\cos\alpha_m + c_p^2(\theta_m)\cos\alpha_k]\\
&\quad + K_a[c_p^2(\theta_k)c_p^2(\theta_m)(\cos\alpha_m + \cos\alpha_k)\\
&\quad - c_p^4(\theta_k)\cos\alpha_m - c_p^4(\theta_m)\cos\alpha_k]\},\\
A_{12} &= 4d\{K_{km}^2[c_p^2(\theta_k)\sin\alpha_m + c_p^2(\theta_m)\sin\alpha_k]\\
&\quad + K_a[c_p^2(\theta_k)c_p^2(\theta_m)(\sin\alpha_m + \sin\alpha_k)\\
&\quad - c_p^4(\theta_k)\sin\alpha_m - c_p^4(\theta_m)\sin\alpha_k]\},\\
A_{13} &= 4h\,[c_p^2(\theta_m) - c_p^2(\theta_k)]\\
&\quad \times\{K_{km}^2 - k_a[c_p^2(\theta_k) + c_p^2(\theta_m)]\},\\
A_{14} &= K_{km}^4 + k_a^2[c_p^2(\theta_k) - c_p^2(\theta_m)]^2\\
&\quad - 2k_aK_{km}^2[c_p^2(\theta_k) + c_p^2(\theta_m)],
\end{aligned}
\tag{11}
$$

where

$$
K_{km} \equiv \Delta t_p(k,m)\, c_p(\theta_k)\, c_p(\theta_m),
$$

$$
k_a \equiv h^2 + R^2 + d^2,
$$

and $k,m = 1,\ldots,N$, where $N =$ the total number of sensors (mounted on one surface). Here, R is the projected radius between the source and the center of the circular array of sensors whose radius is d as shown in Fig. 3.

There are a total of N^2 equations in Eq. (10). To solve this overdetermined system, the Euclidean functional $F(\mathbf{x}^S) = \Sigma_i \Psi^2(\mathbf{x}^S)$ is defined and then minimized by using a modified Newton–Raphson algorithm.[18,20] Equation (10) represents a system of transcendental equations in which each of the coefficients A_i, $i = 1,\ldots,14$, listed in Eqs. (11) is linked through the wave speeds to the unknown source coordinates.

To obtain additional insight into this, we consider the two-dimensional case for which the quasilongitudinal wave speeds are given by Eq. (8) when the direction of wave propagation θ, as given in Eq. (9), is a function of the unknowns x_1^S and x_2^S through a complicated combination of circular and Pythagorean functions. This clearly shows the transcendental nature of Eq. (10). To work out the minimization process of the functional, one needs to compute its gradient and the Hessian matrix, which are given by

$$
\begin{aligned}
\frac{\partial F(\mathbf{x}^S)}{\partial x_i^S} &= 2\Psi(\mathbf{x}^S)\,\frac{\partial \Psi(\mathbf{x}^S)}{\partial x_i^S},\\
\frac{\partial^2 F(\mathbf{x}^S)}{\partial x_i^S \partial x_j^S} &= 2\Psi(\mathbf{x}^S)\,\frac{\partial^2 \Psi(\mathbf{x}^S)}{\partial x_i^S \partial x_j^S}\\
&\quad + 2\left(\frac{\partial \Psi(\mathbf{x}^S)}{\partial x_i^S}\right)\left(\frac{\partial \Psi(\mathbf{x}^S)}{\partial x_j^S}\right),
\end{aligned}
\tag{12}
$$

where $i,j = 1,2,3$. Then, the unknown source coordinates can be determined according to the iterative scheme

$$
x_i^S|_{(n+1)} = x_i^S|_{(n)}\left(\frac{\partial^2 F(\mathbf{x}^S)|_{(n)}}{\partial x_i^S \partial x_j^S}\right)^{(-1)}\left(\frac{\partial F(\mathbf{x}^S)|_{(n)}}{\partial x_i^S}\right),
\tag{13}
$$

where $i,j = 1,2,3$ and where $(\ )^{(-1)}$ represents the inverse matrix.

The principal difference of the above convergence scheme with the regular Newton–Raphson method is that the coefficients in Eq. (11) are scalar fields and must be recalculated after each convergence of Eq. (13), which in turn means that the system of equations, Eqs. (10), is solved several times, until stationary values for the coefficients are obtained; i.e., convergence of the unknown source coordinates is found.

II. NUMERICAL SIMULATIONS

A. Two-dimensional case: Propagation in principal planes

When considering a thin plate, i.e., $d \gg 2h$ and/or $R \gg 2h$, and when the third coordinate x_3^S is fixed to be $x_3^S = -h$, or $= +h$, one might simplify the complete three-dimensional problem to a far simpler case in which (1) sensors need only to be mounted on one surface of the structure, and (2) the wave propagation is restricted to be in the principal plane (1,2). In such a case, Eq. (4) can be rewritten as

$$
\begin{aligned}
\Delta t_p(k,m) &= [c_p(\theta_k)]^{-1}\sqrt{h_1^2 + l_k^2}\\
&\quad - [c_p(\theta_m)]^{-1}\sqrt{h_1^2 + l_m^2},
\end{aligned}
\tag{14}
$$

where $k,m = 1,\ldots,N$ and $k \neq m$. For convenience the thickness of the plate has been redefined as h_1 rather than $2h$ and where $c_p(\theta_k)$ and $c_p(\theta_m)$ are given by Eqs. (8) and (9). There are

$$
\binom{2}{N} = \frac{N!\,2!}{(N-2)!}
$$

such equations.

For the in-plane problem, only four elastic constants, i.e., C_{11}, C_{22}, C_{12} and C_{66}, are needed. The system of Eqs. (10) then simplifies to the set of quadratic transcendental equations:

$$
\begin{aligned}
\phi(\mathbf{x}^S) &= B_1(x_1^S)^2 + B_2(x_2^S)^2 + B_3x_1^Sx_2^S + B_4\,x_1^S\\
&\quad + B_5x_2^S + B_6 \simeq 0,
\end{aligned}
\tag{15}
$$

where

$$B_1 = A_6, \quad B_2 = A_7, \quad B_3 = A_8,$$
$$B_4 = A_{11}, \quad B_5 = A_{12}, \quad B_6 = A_{14}.$$

It should be noted that the method extends to the two other principal planes (1,3) and (2,3) of the orthorhombic symmetry, and to other systems of symmetry by performing a circular permutation on the stiffness coefficients.[21] These operations are summarized in Table I. For other systems of symmetry there are either no analytical expressions for the wave speed curves, even in principal planes, or they may be given by equations which differ from Eq. (8), and these can be found in several texts.[17,22]

B. Numerical results

The parameters used during the numerical simulation are compiled in Table II. The elastic constants used in the simulation were those for a uniaxial fiberglass epoxyde resin composite material.[21] To simulate the influence of random errors on the time-of-flight data, a perturbation procedure has been employed using a quasinormal density of distribution. Next, the algorithm was run ten different times for a given set of parameters. For statistical purposes, averages, standard deviations, and coefficients of variation were computed. Numerical results obtained for three different cases are presented. In Table III are listed the results obtained when the convergence of the algorithm was tested for various locations of the AE source. Beyond the angular dependence of $\Delta R/R$ and $\Delta\alpha$ at a given R, which may change for other sets of the parameters, it is seen that there is a dramatic decrease in the accuracy of the location process when the source is located exterior to the array of sensors. This trend is significant, as it remains unchanged for other combinations of the parameters. The difficulty in recovering the source location is shown by the increase of the number of iterations required from just a few at $R = 5.00$ cm to several tens when $R = 15.00$ cm. This clearly shows the impediments at convergence of the noisy data when the source is situated far from the center of the array of sensors. In the numerical simulations it was found that the algorithm usually did not converge for the two-dimensional source-location problem with $R > 50.00$ cm. In Table IV are listed the results about the influence of the number of sensors, while in Table V are the results of the role of systematical errors on the values of the elastic constants on the recovered coordinates of the AE source.

TABLE II. Parameters of the 2-D numerical simulation.

$d = 10.00$ cm
R = variable in Table III, $= 5.00$ cm in Tables IV and V
α = variable in Table III, from 0° to 90° with a 10° angular step, $= 45°$ in Tables IV and V
$h = 0.01$ cm
$n = 8$ in table III, variable in Table IV, $= 4$ in Table V
$d(\Delta t_p) = 1\%$ in Table III, $= 2\%$ in Table IV, $= 0\%$ in Table V
$\rho = 2.108$ g/cm^3
$C_{11} = 26.30$ GPa
$C_{22} = 65.50$ GPa
$C_{12} = 9.58$ GPa
$C_{66} = 10.50$ GPa

C. Extension to the three-dimensional problem

The full three-dimensional source-location problem is much more challenging than its two-dimensional counterpart, as the determination of the X_3 coordinate (or x_3^S, i.e., the location across the thickness of the structure) is possible that way. Applications to detect and locate defects in composite materials are of special importance. Nevertheless, to solve the problem, one needs to return to the general solution given in the first section. By performing extensive numerical simulations, it has been possible to clearly show that the convergence is extremely difficult with noise-corrupted data when the sensors are distributed over only one surface of the structure, on either the top or bottom surfaces. Such a testing situation may preclude a correct convergence, as there is nonuniqueness of the recovered source location. For example, if the measurements are made with a circular array on an isotropic solid, it is obvious that any position along the axis of the circle yields the same source-location result. More generally, the $+x_3^S$ and the $-x_3^S$ coordinates of the source lead to an identical result. Despite that inherent restriction, there is a simple solution to the three-dimensional problem, which may, albeit, not always be practical, that is, by mounting the sensors on both sides of the plate, as was described in the previous section. The algorithm defined in this manner can be extremely efficient. Some results obtained by using a numerical simulation are introduced in the following subsection.

TABLE I. Circular permutations on stiffness coefficients.

System	Orthorhombic[a]			Hexagonal[a,b]		Tetragonal[c]		Cubic[a]	Isotropic[d]
Plane	(1,2)	(1,3)	(2,3)	(1,2)	(*,3)[e]	(1,2)	(*,3)[e]	(C)[f]	(I)[g]
	C_{11}	C_{11}	C_{22}	C_{11}	C_{11}	C_{11}	C_{11}	C_{11}	C_{11}
	C_{22}	C_{33}	C_{33}	C_{11}	C_{33}	C_{11}	C_{33}	C_{11}	C_{11}
	C_{66}	C_{55}	C_{44}	C_{66}	C_{44}	C_{66}	C_{44}	C_{44}	C_{44}
	C_{12}	C_{13}	C_{23}	C_{12}	C_{13}	C_{12}	C_{13}	C_{12}	C_{12}

[a] For all classes of symmetry.
[b] With for plane (1,2) $A = 2C_{66}/(C_{11} - C_{12}) = 1$.
[c] For Hermann–Mauguin classes of symmetry 422, $4mm$, $\bar{4}2m$, $4/mmm$.
[d] With $A' = 2C_{44}/(C_{11} - C_{12}) = 1$.
[e] (*,3) = Any plane of propagation comprising axis 3.
[f] (C) Propagation in a cube face.
[g] (I) Propagation in any plane.

TABLE III. Algorithm convergence for various source locations.

	$R = 5.00$ cm		$R = 10.00$ cm		$R = 15.00$ cm	
α(deg)	$\Delta R/R(\%)$	$\Delta\alpha$(deg)	$\Delta R/R(\%)$	$\Delta\alpha$(deg)	$\Delta R/R(\%)$	$\Delta\alpha$(deg)
0	0.146	0.183	0.324	0.232	1.523	0.529
10	0.170	0.100	0.306	0.140	2.414	0.485
20	0.150	0.189	0.311	0.174	2.709	0.713
30	0.138	0.163	0.349	0.138	2.692	0.550
40	0.122	0.096	0.338	0.149	1.499	0.293
50	0.114	0.059	0.467	0.113	2.329	0.372
60	0.236	0.072	0.309	0.101	2.400	0.256
70	0.350	0.046	0.225	0.047	0.502	0.051
80	0.204	0.120	0.159	0.026	0.687	0.087
90	0.242	0.244	0.091	0.049	2.094	0.049

D. Numerical simulation results

To describe this problem in a very general way, a material whose elastic properties possess an orthorhombic symmetry has been considered. The mechanical parameters used during the numerical simulation are listed in Table VI. The elastic constants were measured for a tropical wood[23] by use of an advanced ultrasonic spectro-interferometer.[24] Some significant results of the numerical simulation are listed in Tables VII–X. From these results one can emphasize the following general features: (1) For R and α, the convergence is extremely good in the three-dimensional case compared to the two-dimensional one. Also, the number of iterations is surprisingly very stable in this case, requiring usually only five to seven. (2) The reduction in the accuracy of recovering R and α when increasing R as noted in Sec. II B is less drastic in the three-dimensional case. This is seen if one compares the third column of Table VII with the fourth entry of Table III. The convergence for R and α in the three-dimensional problem remains excellent at $R = 50.0$ cm, whereas there is not even convergence for the 2-D case as was noted previously. (3) Unfortunately, the convergence for x_3^S is not as good as for R or α. When increasing R, the drop of accuracy for the recovered source coordinate x_3^S is considerable going from 1 to 7 when modifying R from $R = 5.00$ to 50.00 cm versus a change from 1 to 2 in terms of R. Thus, to obtain an acceptable accuracy for the determination of x_3^S, a very stringent precision on the time delay measurements is required, something in the range of a few ns to achieve a 1% accuracy of the location. (4) The influence of other parameters such as the value of x_3^S or the orientation of the principal axes, and therefore the values of the elastic constants in any given direction, is of considerable importance as the results tabulated in Tables IX and X show. Nevertheless, the variations in the results appear to be far smaller when compared to the influence of other variables such as the range R or N, the number of sensors.

III. EXPERIMENTAL RESULTS FOR A UNIDIRECTIONAL COMPOSITE

A. Sample description

The samples used in the experimental work were fiberglass-reinforced materials from the Extren 500 series,[25] which were made with an isophthalic polyester resin. This type of material is generally used in structural applications involving corrosive environments and is manufactured by the pultrusion process. The final product is porous and has a medium homogeneity as well as rough surfaces. These features add some inherent obstacles to the source-location process, which are related to dispersion and attenuation of the elastic waves propagated in this material.

Plates that were 304.8 mm square and of thickness 6.35 mm were tested. The glass fibers lay in the plane (1,2) and were mainly oriented along one principal direction, say in the direction X_1. Thus these composite materials are to a good approximation unidirectional. The ratio of the Young moduli in the two principal in-plane directions (e.g., X_1 and X_2) was approximately 1.5.

TABLE IV. Algorithm convergence for different numbers of sensors.

		$\bar{x}$	σ_x	$c_x = (\sigma_x/\bar{x})$ (%)
$n = 4$	R	5.010	0.044	0.88
	α	44.891	0.308	0.67
$n = 8$	R	4.997	0.013	0.26
	α	45.013	0.228	0.51
$n = 16$	R	5.004	0.008	0.16
	α	45.030	0.073	0.16

TABLE V. Influence of systematical errors on stiffness coefficients on the algorithm convergence.

		$\Delta R/R(\%)$	$\Delta\alpha/\alpha(\%)$
$C11$	+ 10%	+ 1.78	− 3.06
	− 10%	− 1.55	+ 3.32
$C22$	+ 10%	+ 2.52	+ 3.71
	− 10%	− 1.79	− 4.68
$C12$	+ 10%	+ 0.87	− 0.75
	− 10%	− 0.86	+ 0.77
$C66$	+ 10%	+ 2.21	− 1.80
	− 10%	− 2.22	+ 2.05

TABLE VI. Parameters of the 3-D numerical simulation.

$d = 10.00$ cm
R = variable in Table VIII, = 15.00 cm in Tables IX–XI
$\alpha = 30.00°$
$h = 2.00$ cm
$n = 8$ in Tables VIII, X, and XI, variable in Table IX
$d(\Delta t_p) = 1\%$
$\rho = 1.280$ g/cm^3
$C_{11} = 7.45$ GPa
$C_{22} = 8.30$ GPa
$C_{33} = 29.30$ GPa
$C_{44} = 2.88$ GPa
$C_{55} = 2.71$ GPa
$C_{66} = 1.65$ GPa
$C_{12} = 4.36$ GPa
$C_{13} = 3.97$ GPa
$C_{23} = 4.97$ GPa

TABLE VIII. Algorithm convergence for different numbers of sensors.

		$\bar{x}$	σ_x	$c_x = (\sigma_x/\bar{x})$ (%)
	R	15.001	0.020	0.13
$n = 8$	α	30.026	0.149	0.50
	Z	1.028	0.127	12.36
	R	15.001	0.015	0.10
$n = 16$	α	29.962	0.043	0.14
	Z	1.111	0.041	3.66
	R	14.999	0.005	0.03
$n = 32$	α	29.984	0.033	0.11
	Z	1.004	0.019	1.90

B. System measurements

To test the two-dimensional version of the algorithm, an ultrasonic *point-source/point-receiver* materials testing system was used.[26,27] Such a system has been used with considerable success to determine the frequency-dependent wave speeds and attenuations of a material. A convenient simulated acoustic emission source is the fracture of a glass capillary, 0.05-mm i.d. and 0.08-mm o.d. The rise time of the resulting step force excitation is typically about 50 ns. The sensors used here are wide bandwidth piezoelectric transducers whose aperture was 1.3 mm. The detected acoustic emission signals were amplified 60 dB with broadband preamplifiers and recorded on transient recorders operating with sampling rates ranging 1–60 MHz with 10-bit resolution. Four recording channels were typically used to make the measurements. Although the minimum number of sensors for a two-dimensional source-location determination is three, for practical reasons, the same sensors were used both for the source-location determination and for the calibration of the material anisotropy which is discussed in the next subsection.

C. Calibration procedure

Unidirectional composite materials are properly described by a hexagonal symmetry. They are elastically transversely isotropic whose properties are fully specified with five independent elastic constants. Because the discussion is restricted to the two-dimensional case and to measurements made on the principal plane (1,2), only four elastic constants, C_{11}, C_{22}, C_{12}, and C_{66}, need to be determined. These moduli are determined from measurements along a few particular directions of propagation. The results are

$$(C_{11}/\rho) = c_{p1}^2, \quad (C_{22}/\rho) = c_{p2}^2, \quad (C_{66}/\rho) = c_S^2, \tag{16}$$

$$C_{12} = \{[2\rho c_{45}^2 - (C_{11} + C_{22})/2 - C_{66}]^2 - [(C_{11} - C_{22})/2]^2\}^{1/2} - C_{66}, \tag{17}$$

where c_{p1} and c_{p2} are the wave speeds of the longitudinal waves along the principal axes 1 and 2, c_S is the wave speed of the transverse wave along the principal axes 1 or 2, and c_{45} is the wave speed of the quasilongitudinal wave along the diagonal axes D_1 and D_2, i.e., at ± 45 deg; ρ is the density of the material.

To determine the required wave speeds as precisely as possible, several measurements were performed by breaking the glass capillary tubes in numerous referenced locations along the axes of interest, as shown in Fig. 4. The longitudinal wave speeds were determined by simple chronometry on the recorded waveforms. The shear wave speed c_S was estimated by other means. The results of the measurements were

$$c_{p1} = 0.377 \text{ cm}/\mu\text{s}, \quad c_{p2} = 0.335 \text{ cm}/\mu\text{s},$$

$$c_S = 0.175 \text{ cm}/\mu\text{s}, \quad c_{45} = 0.346 \text{ cm}/\mu\text{s}.$$

We note that the density of the material is not required if

TABLE VII. Algorithm convergence for various source locations.

		$\bar{x}$	σ_x	$c_x = (\sigma_x/\bar{x})$ (%)
	R	49.960	0.090	0.18
$R = 50$ cm	α	30.036	0.132	0.44
	Z	1.160	0.406	35.02
	R	15.001	0.020	0.13
$R = 15$ cm	α	30.026	0.149	0.50
	Z	1.028	0.127	12.36
	R	4.998	0.005	0.09
$R = 5$ cm	α	30.061	0.118	0.39
	Z	0.992	0.049	4.91

TABLE IX. Algorithm convergence function of the Z position.

		$\bar{x}$	σ_x	$c_x = (\sigma_x/\bar{x})$ (%)
	R	14.999	0.017	0.11
$Z = 0.5$ cm	α	30.042	0.110	0.37
	Z	0.497	0.123	24.71
	R	15.001	0.020	0.13
$Z = 1.0$ cm	α	30.026	0.149	0.50
	Z	1.028	0.127	12.36
	R	14.991	0.017	0.12
$Z = 1.5$ cm	α	30.075	0.122	0.41
	Z	1.357	0.146	10.76

TABLE X. Algorithm convergence function of the material orientation.

		$\bar{x}$	σ_x	$c_x = (\sigma_x/\bar{x})$ (%)
$n_i = n_1$	R	15.015	0.047	0.31
	α	30.058	0.127	0.42
	Z	1.016	0.077	7.61
$n_i = n_2$	R	15.012	0.049	0.33
	α	29.934	0.282	0.94
	Z	1.087	0.071	6.53
$n_i = n_3$	R	15.001	0.020	0.13
	α	30.026	0.149	0.50
	Z	1.028	0.127	12.36

a source of acoustic emission is to be located. The procedure is described in the following section.

D. Isotropic and anisotropic optimizations

When the calibration procedure is completed, one can proceed with the source-location process. This is illustrated here by using the fracture of a glass capillary as a simulated AE surce at an arbitrary source location. The advantages of this source include its broad bandwidth, high excitation energy, and unidirectional radiation characteristics. From the recorded transient waveforms, the start of the detected signals at the different stations are referenced. A set of characteristic waveforms is shown in Fig. 5. From these, differences in the time of flight of the quasilongitudinal wave arrivals, $\Delta t_p\,(km)$, i.e., terms of Eq. (13), are computed, and the recovery of the location of the simulated source location is made through the simplified two-dimensional version of the optimization algorithm. To ascertain if the results would differ if the material was elastically isotropic and anisotropic, the algorithm was run twice, using for the isotropic case, the supplementary relationships

$$C_{22} = C_{11}, \quad C_{66} = (C_{11} - C_{12})/2. \tag{18}$$

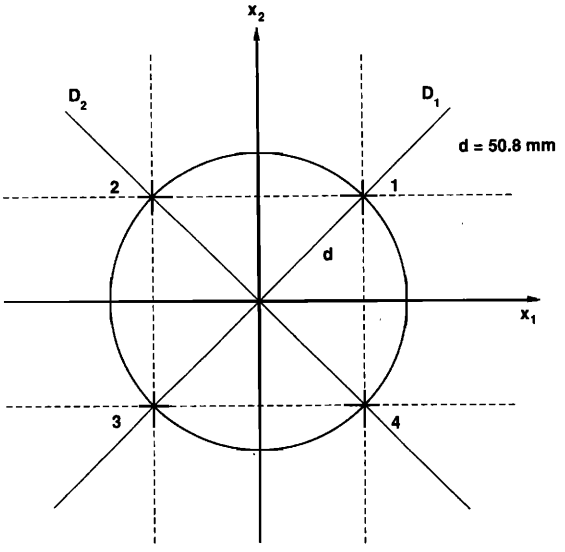

FIG. 4. Geometry for the calibration procedure.

Some experimental results are collected in Table XI for 12 different locations, all of them situated in the upper right quadrant of Fig. 4. These results clearly show that the localization of the pointlike acoustic emission source is correctly done in most of the cases. Furthermore, the results are systematically better when the material is assumed to be transversely isotropic instead of isotropic. It is noted that, in some cases, there is no convergence when the material was assumed to be isotropic. Generally, the convergence is more precise when the source is located inside of the circular array of sensors, as shown in the last four entries of Table XI. This trend is in agreement with the results obtained by using the two-dimensional numerical simulation (Table III). On the other hand, for some locations, far removed from the center of the array (e.g., the first three entries in Table XI), the convergence may be difficult to obtain. In such a case, corrections must be included in the treatment of the data to insure a proper convergence. For these remote areas, several factors are detrimental to the accuracy of the recovered source location. These include the pronounced geometric dispersion of the signals and the attenuation and dissipation of the bulk modes, as shown in Fig. 5. The amplitude of the quasilongitudinal bulk mode is negligible when compared to the Lamb waves,[28] especially for sensors in the farfield of a source where the signal strength of the bulk modes are of small amplitude or vanish.[29,30]

Other limitations exist as well. Some of these are a consequence of the simplifications associated with the two-dimensional representation of the problem, while others are related to the instrumentation that has been used. A waveform digitizer operating at 3 MHz provides a 0.3-μs time resolution over a characteristic 30-μs time delay difference, or 1% uncertainty of presision. In such a case, when four sensors are used, and when $R \simeq 2d$, corresponding to the first three entries in Table XI, the errors in the source-location process might be as high as 5% or worse as was shown in Ref. 15.

Although the simulated source has been kept distant from any sensor, the propagation of the elastic waves, during the calibration procedure as well as during the source-location process, occurs in nonprincipal planes. Hence, in a correct procedure, one should include the two remaining elastic constants, C_{13} and C_{44}, with $C_{44} = (C_{11} - C_{13})/2$ and compute the eigenvalues of the Green–Christoffel tensor, as was done for the full three-dimensional problem.

IV. CONCLUSIONS

We have described in this paper a procedure for finding an efficient solution to the problem of locating a source of acoustic emission in an anisotropic plate. In some cases, which were demonstrated with experiments, the source-location problem can be treated as a two-dimensional situation. However, in the more general case, a more realistic approach is to deal with the full three-dimensional problem, which implies several restrictions. These include the following. (1) The measurements are made in a homogeneous, elastic solid. (2) The directions of the principal acoustic axes in the specimen must be known *a priori*, and knowledge of the elastic constants must be known or determined in a cali-

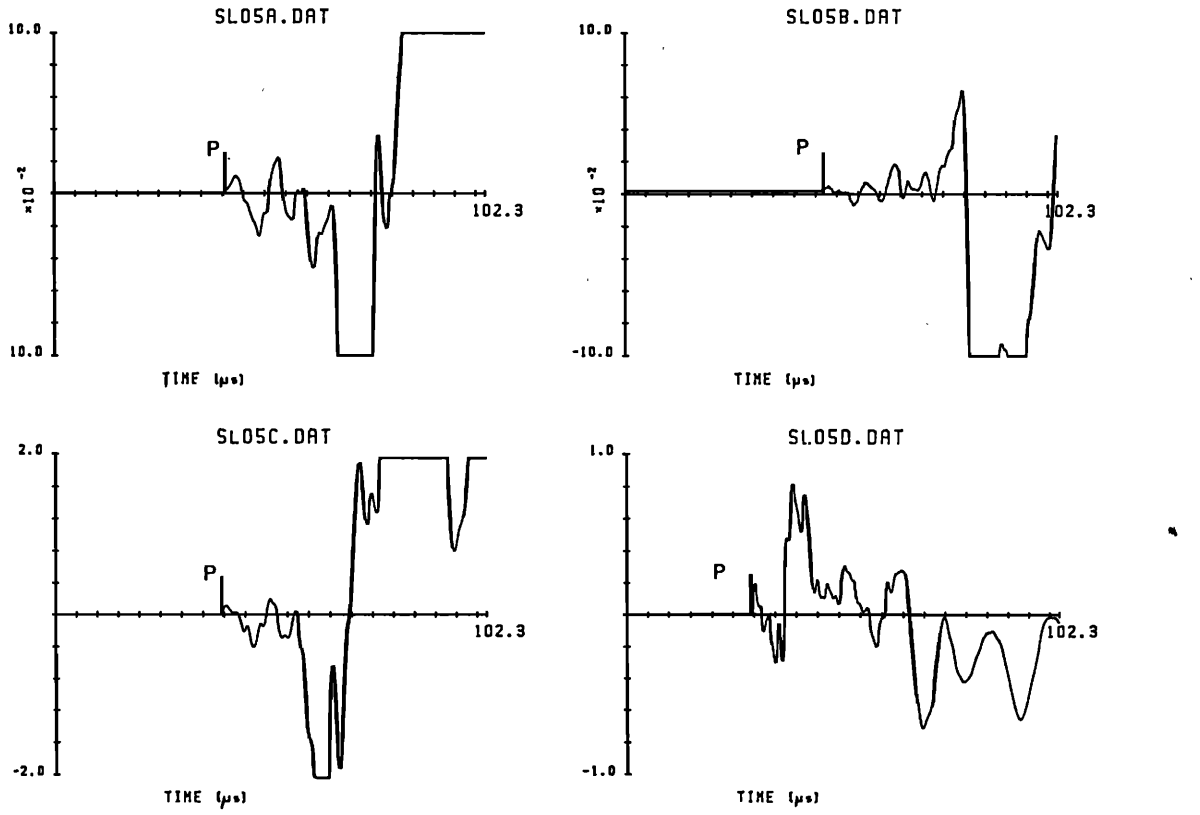

FIG. 5. Set of detected waveforms—fiberglass/epoxy specimen.

bration experiment. (3) When the propagation is in nonprincipal planes, the eigenvalues of the Green–Christoffel tensor must be determined to obtain the wave speeds of the quasimodes. (4) The differences of time delays of particular wave modes must be accurately determined. The requirements are for these to be measured to within 0.1 μs when only the range of the source and its orientation in a plane are sought. The time differences need to be measured with ns resolution when the third coordinate of a source is to be determined. Despite the above restrictions and limitations, the method we have described is expected to be useful for monitoring the progression of failure in a composite structure.

Extensions of this work will include its application to other specimen geometries, as well as other sensor distributions. Of special interest might be the two orthogonal lines of sensors geometry. For location of pointlike AE sources in very thin plates or in thin layers, numerical schemes similar to those described in this paper may be based on arrival time data of Lamb waves, pseudo-Rayleigh, or Love waves. A reliable solution of the three-dimensional source-location problem is best obtained from measurements in thick plates. That is, it is not possible to reliably determine the through-thickness coordinate of an AE source in a very thin layer, that is, one which is only a few μm thick.

TABLE XI. Experimental results—comparison of the convergence for anisotropic/isotropic hypothesis.

Real position		Anisotropic		Isotropic	
R(mm)	α(deg)	R(mm)	α(deg)	R(mm)	α(deg)
107.77	45.00	116.13	43.42	Divergence	
91.58	33.69	90.44	29.09	85.28	28.59
91.58	56.31	91.04	53.84	Divergence	
80.32	18.44	87.70	14.09	67.76	16.90
80.32	71.56	81.31	67.38	Divergence	
76.20	0.00	80.08	0.12	59.78	0.15
76.20	90.00	86.21	88.16	186.41	88.17
71.84	45.00	66.98	44.45	Divergence	
50.80	0.00	53.67	0.07	43.95	0.09
50.80	90.00	51.34	88.94	69.10	89.47
25.40	0.00	25.59	0.15	22.91	0.21
25.40	90.00	25.68	89.20	30.84	89.47

ACKNOWLEDGMENTS

We acknowledge the support of the National Science Foundation through a grant to the Materials Science Center of Cornell University. Portions of this work were also supported by the Office of Naval Research (Physics Program). We also thank Robert M. Emerson from Joseph T. Ryerson & Son Inc. (Chicago, IL) for his kind collaboration in providing us materials to test and for giving us authorization to publish the results.

[1]K. Aki and P. G. Richards, *Quantitative Seismology* (Freeman, San Francisco, 1980), Vol. 1, pp. 383–477.

[2]C. B. Scruby, R. J. Dewhurst, D. A. Hutchins, and S. B. Palmer, "Laser generation of ultrasound in metals," in *Research Techniques in Nondestructive Testing*, edited by R. S. Sharpe (Academic, New York 1982), Vol. 5, pp. 281–327.

[3]J. A. Baron and S. P. Ying, "Acoustic emission source location," in *Nondestructive Testing Handbook* (ASNT, Columbus, OH, 1987), Vol. 5, Sec. 6, pp. 136–154.
[4]A. Tobias, "Acoustic-emission source location in two dimensions by an array of three sensors," Nondest. Test. Int. **10**, 9–12 (1976).
[5]M. Asty, "Acoustic emission source location on a spherical or plane surface," Nondest. Test. Int. **12**, 223–226 (1978).
[6]Y. H. Pao, "Theory of acoustic emission," in *Elastic Waves and Nondestructive Testing of Materials*, AMD Vol. 29, edited by Y. H. Pao (ASME, New York, 1978), pp. 107–127.
[7]I. Grabec, "Application of correlation techniques for localization of acoustic emission sources," Ultrasonics **16**, 111–115 (1978).
[8]R. N. Bracewell, *The Fourier Transform and Its Applications* (McGraw–Hill, New York, 1986), pp. 98–123.
[9]P. N. Hsieh, "Quantitative Acoustic Emission Source Characterization in an Aluminum Specimen," Ph.D. dissertation, Cornell University, Ithaca, NY, 1987.
[10]W. Sachse and S. Sancar, "Acoustic emission source location on plate-like structures using a small array of transducers," U.S. Patent No. 4,592,034 (1986).
[11]G. C. Carter, "Passive ranging errors due to receiving hydrophone position uncertainty," J. Acoust. Soc. Am. **65**, 528–531 (1979).
[12]C. S. Clay, M. J. Hinich, and P. Shaman, "Error analysis of velocity and direction measurements of plane waves using thick large-aperture arrays," J. Acoust. Soc. Am. **53**, 1161–1166 (1973).
[13]C. S. Clay and M. J. Hinich, "Use of a two-dimensional array to receive an unknown signal in a dispersive waveguide," J. Acoust. Soc. Am. **47**, 435–440 (1970).
[14]S. P. Ying, D. R. Hamlin, and D. Tanneberger, "A multichannel acoustic emission monitoring system with simultaneous multiple event data analyses," J. Acoust. Soc. Am. **55**, 350–356 (1974).
[15]B. Castagnede, W. Sachse, and K. Y. Kim, "Optimization de la localisation d'une source ponctuelle d'émission acoustique dan un matériau anisotrope homogène," C. R. Acad. Sci. (Paris) II **307**, 1473–1478 (1988).
[16]B. Castagnede, W. Sachse, and K. Y. Kim, "Localisation de sources d'émission acoustique dan un matériau composite," C. R. Acad. Sci. (Paris) II **307**, 1595–1600 (1988).
[17]B. A. Auld, *Acoustic Fields and Waves in Solids* (Wiley, New York, 1973), Vol. 1.
[18]P. G. Ciarlet, *Introduction à l'analyse numérique matricielle et à l'optimisation* (Masson, Paris, 1982), pp. 167–207.
[19]W. H. Press, B. P. Flannery, S. A. Teukolsky, and W. T. Vetterling, *Numerical Recipes. The Art of Numerical Computing* (Cambridge U. P., New York, 1986), pp. 240–269.
[20]B. Hosten and B. Castagnede, "Optimization of the computation of elastic constants from the measurements of ultrasonic velocities," C. R. Acad. Sci. (Paris) II **296**, 297–300 (1983).
[21]B. Castagnede, "Mesures des constantes élastiques de solides anisotropes par une méthode ultrasonore," Ph.D. thesis, University of Bordeaux I, 1984.
[22]E. Dieulesaint and D. Royer, *Ondes élastiques dan les solides* (Masson, Paris, 1974), pp. 113–166.
[23]B. Hosten and B. Castagnede, "Measurements of elastic constants of wood by means of numerical ultrasonic interferometry and their optimization," C. R. Acad. Sci. (Paris) II **296**, 1761–1764 (1983).
[24]J. Roux, B. Hosten, B. Castagnede, and M. Deschamps, "Mechanical characterization of solids by ultrasonic spectro-interferometry," Rev. Phys. Appl. **20**, 351–358 (1985).
[25]*Technical Booklet on Fiber Glass Reinforced Materials*, Extren 500 Series (Ryerson, Plastics Division, Chicago, 1987).
[26]W. Sachse and K. Y. Kim, "Point-source/point-receiver materials testing," in *Review of Quantitative Non-destructive Evaluation*, edited by D. O. Thompson and D. E. Chimenti (Plenum, New York, 1986), Vol. 6A, pp. 311–320.
[27]W. Sachse and K. Y. Kim, "Quantitative acoustic emission and failure mechanics of composite materials," Ultrasonics **25**, 195–203 (1987).
[28]Y. H. Pao and R. K. Kaul, "Waves and vibrations in isotropic and anisotropic plates," in *R. D. Mindlin and Applied Mechanics*, edited by G. Hermann (Pergamon, New York, 1974).
[29]A. N. Ceranoglu and Y. H. Pao, "Propagation of elastic pulses and acoustic emission in a plate," ASME J. Appl. Mech. **48**, 125–147 (1981).
[30]R. L. Weaver and Y. H. Pao, "Axisymmetric elastic waves excited by a point source in a plate," ASME J. Appl. Mech. **49**, 821–836 (1982).